

4. J. Gossler and R. Kind, *Earth Planet. Sci. Lett.* **138**, 1 (1996).
5. P. M. Shearer, *Geophys. J. Int.* **115**, 878 (1993).
6. N. Wajeman, *Geophys. Res. Lett.* **15**, 669 (1988).
7. E. Ito and E. Takahashi, *J. Geophys. Res.* **94**, 10637 (1989).
8. T. Duffy and D. L. Anderson, *ibid.*, p. 1895.
9. T. Infune, *Phys. Earth Planet. Inter.* **45**, 324 (1987).
10. *PP* is a *P* wave that reflects once from Earth's surface. *P'P'* (*PKPPK*) is like *PP* but travels through the core. *PzP* are underside reflections, where *z* is the depth of the reflection (for example, *P660P* is a *P* wave reflected from a depth of 660 km). *Pdzd* are topside reflections where *d* is either *p* or *s* (for example, *Ps660p* is a *P* wave with a source- or receiver-side *S-P* reflection-conversion).
11. H. M. Benz and J. E. Vidale, *Nature* **365**, 147 (1993).
12. N. Petersen *et al.*, *Geophys. Res. Lett.* **20**, 859 (1993); M. G. Bostock, *ibid.* **23**, 1593 (1996).
13. L. Vinnik, G. Kosarev, N. Petersen, *ibid.*, p. 1485.
14. A. C. Lees, M. S. T. Bukowski, R. Jeanloz, *J. Geophys. Res.* **88**, 8145 (1983).
15. U. R. Christensen and D. A. Yuen, *ibid.* **89**, 4389 (1984).
16. R. van der Hilst, E. R. Engdahl, W. Spakman, *Geophys. J. Int.* **115**, 264 (1993).
17. U. Christensen, *Earth Planet. Sci. Lett.* **140**, 27 (1996); H.-P. Bunge, M. A. Richards, J. R. Baumgardner, *Nature* **379**, 436 (1996); P. J. Tackley, D. J. Stevenson, G. A. Glatzmaier, G. Schubert, *J. Geophys. Res.* **99**, 15877 (1994).
18. The data were provided by IRIS-Seattle (Incorporated Research Institutions for Seismology) as FARM (fast archive recovery method) data volumes.
19. We calculated the SNR from the peak-to-peak amplitude (PTPA) 65 to 5 s before the predicted *PP* arrival time versus the PTPA from the *PP* time to 60 s after, using the band-pass-filtered seismograms (10 to 50 s).
20. K. Stammler, *Comput. Geosci.* **19**, 135 (1993). The data were detrended and filtered with a causal three-pole bandpass filter between 3 and 50 s before deconvolution and filtered again with a three-pole acausal bandpass filter between 10 and 50 s to shift the weighting toward longer periods. The acausal filter produced symmetric side lobes, which appeared in the synthetics (Fig. 1B, appearing ~60 s before *P* and *PKP*) but not in the data. The stacking procedure apparently canceled out this effect when applied to the data because of the sheer number of events. The *PP* phase was deconvolved from the entire seismogram to account for varying source-time histories and radiation patterns. To enhance the amplitude of the precursors to *PP*, we aligned the seismograms on the resulting spike and slant-stacked (stacking along a travel-time curve) to obtain the slownesses (inverse of apparent velocity) of the *PP* phase and its precursors (1).
21. International Association of Seismology and the Physics of the Earth's Interior [B. L. N. Kennett and E. R. Engdahl, *Geophys. J. Int.* **105**, 429 (1991)]. Attenuation Q^{-1} is from the Preliminary Reference Earth Model [A. M. Dziewonski and D. L. Anderson, *Phys. Earth Planet. Inter.* **25**, 297 (1981)]. Density is from AK135 [B. L. N. Kennett, E. R. Engdahl, R. Buland, *Geophys. J. Int.* **122**, 108 (1995)].
22. F. Neele, H. de Regt, J. VanDecar, in preparation.
23. $V_p = \sqrt{(\lambda + 2\mu)/\rho} = \sqrt{(\kappa + 4\mu/3)/\rho}$, where λ and μ are the Lamé parameters (μ is also known as the shear modulus) and κ is the bulk modulus:

$$\Phi = (\lambda + 2\mu/3)/\rho = \kappa/\rho$$
24. K. Aki and P. Richards, *Quantitative Seismology: Theory and Methods* (Freeman, San Francisco, 1980), vol. 1.
25. J. C. Jaeger, *Elasticity, Fracture, and Flow: With Engineering and Geological Applications* (Chapman and Hall, London, 1969).
26. For waves with a slowness of 7 s degree⁻¹ (*PP* slowness for a distance of 120°), a model for which V_p is constant but V_s and ρ change produces a small *PP*, whereas a model in which V_s and ρ are constant but V_p changes produces a large but negative $\dot{P}\dot{P}$ as compared with IASP91. $\dot{S}\dot{S}$ is significant only when there is a jump in V_s and ρ .
27. J. Ita and L. Stixrude, *J. Geophys. Res.* **97**, 6849 (1992).
28. K. E. Bullen and B. A. Bolt, *An Introduction to the Theory of Seismology* (Cambridge Univ. Press, Cambridge, 1987).
29. R. Kind, *J. Geophys.* **42**, 191 (1976).
30. S. P. Grand and D. V. Helmberger, *Geophys. J. R. Astron. Soc.* **76**, 399 (1984); M. C. Walck, *ibid.*, p. 697; L. E. Jones, J. Mori, D. V. Helmberger, *J. Geophys. Res.* **97**, 8765 (1992).
31. J. R. Bowman and B. L. N. Kennett, *Geophys. J. Int.* **101**, 411 (1990).
32. T. Ryberg *et al.*, *Ann. Geophys.* (abstract) (1996), p. C68.
33. P. Vacher, A. Mocquet, C. Sotin, *ibid.*, p. C41.
34. B. H. Hager and M. A. Richards, *Philos. Trans. R. Soc. London Ser. A* **328**, 309 (1989); A. M. Forte, A. M. Dziewonski, R. J. O'Connell, *Science* **268**, 386 (1995).
35. R. Kind, *J. Geophys.* **45**, 373 (1979).
36. We thank G. Bock, J. Gossler, W. Hanka, F. Krüger, P. Richards, T. Ryberg, C. Scholz, and S. Sobolev for helpful discussions and reviews. We thank IRIS-Seattle for the FARM tapes and contributing stations from the Federation of Digital Seismic Networks. K. Stammler, R. Benson, and T. McSweeney supplied software. Supported by the Deutsche Forschungsgemeinschaft.

23 May 1996; accepted 16 September 1996

Organic Glasses: A New Class of Photorefractive Materials

P. M. Lundquist, R. Wortmann,* C. Geletneky,† R. J. Twieg,‡ M. Jurich, V. Y. Lee, C. R. Moylan, D. M. Burland‡

The performance of amorphous organic photorefractive (PR) materials in applications such as optical data storage is generally limited by the concentration of active molecules (chromophores) that can be incorporated into the host without forming a crystalline material with poor optical quality. In polymeric PR systems described previously, performance has been limited by the necessity of devoting a large fraction of the material to inert polymer and plasticizing components in order to ensure compositional stability. A new class of organic PR materials composed of multifunctional glass-forming organic chromophores is described that have long-term stability and greatly improved PR properties.

The PR effect may be defined as the spatial modulation of a material's refractive index n in response to an optically induced charge distribution. The spatial index modulation may be out of phase with the spatial modulation of the original optical excitation, and this phase shift can induce an exchange of energy between laser beams, which leads to a variety of applications including optical correlators, beam-fanning intensity limiters, and novelty filters (1). Photorefractive materials have also been considered for use as reversible recording media in holographic optical data storage. In addition to large changes in n per unit photon absorbed, most applications require PR media with high optical clarity and minimal light-scattering levels. We report here a new type of PR system based on amorphous organic glasses (2) with substantial improvements in PR and sample-quality properties.

The PR effect was first observed in a LiNbO_3 crystal more than 30 years ago (3).

Polymeric PR materials were initially described in 1991 (4). In the relatively brief intervening period, their performance has improved dramatically (5, 6) to the point where important properties, such as maximum n modulation (Δn) and two-beam coupling (2BC) gain (Γ), actually equal or exceed those of their inorganic counterparts (7). The features required for PR behavior (photocharge generation, photoconductivity, charge trapping, and nonlinear or birefringent optical response) are usually provided by separate components, each of which can be dissolved as a guest in the polymer host or chemically attached to the polymer. Several of the most promising polymeric PR materials containing a charge transport polymer host are designed in this way (8, 9). The largest Δn and Γ previously reported were measured in a mixture of the nonlinear optical chromophore 2,5-dimethyl-4-*p*-nitrophenylazoanisole (DMNPAA) doped into a polyvinylcarbazole (PVK) host polymer with a plasticizer (9-ethylcarbazole, ECZ) and a small quantity of 2,4,7-trinitro-9-fluorenone (TNF) added as a charge-generating photosensitizer (10). Unfortunately, the high concentration (up to 50 weight %) of DMNPAA required to produce the large Δn results in a metastable material system in which the chromophore crystallizes out over time, a process that seriously com-

Almaden Research Center, IBM Research Division, 650 Harry Road, San Jose, CA 95120-6099, USA.

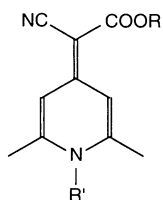
*Present address: Institut für Physikalische Chemie, Johannes Gutenberg-Universität, Jakob Welder-Weg 11, 55099 Mainz, Germany.

†Present address: FB Chemie der Philipps-Universität, Hans-Meerwein-Strasse, 35032 Marburg, Germany.

‡To whom correspondence should be addressed.

promises optical quality (11–13). Many doped polymeric systems share this shortcoming: The PR performance generally increases with increasing chromophore concentration and reaches an upper limit based on the solubility of the chromophore in the host polymer.

We have devised a material design strategy in which the chromophore itself forms a glass and in which the PR effect is not dominated by the Pockels effect, but rather by an orientational enhancement mechanism (14). Fully functionalized polymer systems are another approach to increasing chromophore concentration but require substantially more synthetic effort (6). The PR effect in inorganic crystals involves the linear electrooptic (EO) or Pockels effect wherein the periodic space charge field gives rise to a spatially periodic modulation in n . Early attempts to mimic this mechanism in PR polymers led to the use of chromophores exhibiting large linear EO effects. Chromophores were thus chosen on the basis of their large first hyperpolarizabilities (β) and large ground-state electric dipole moments (μ). However, in polymeric systems with low glass-transition temperatures T_g , spatial modulation of the chromophore orientation in many cases makes the dominant contribution to the observed PR effect (14, 15). In these cases, the birefringence of the chromophore causes a periodic n modulation as the μ s of the chromophores are preferentially aligned in the periodic internal space charge field. As a result of this orientational enhancement effect, the polarizability anisotropy $\delta\alpha = \alpha_{zz} - (\alpha_{xx} + \alpha_{yy})/2$ of a given chromophore is often more important than β (15). Here α_{ii} is the i th diagonal chromophore polarizability tensor element in the molecular coordinate system, with the z -axis being along the molecule's dipole moment vector. The dihydropyridine chromophores described here have large birefringences and μ values but very small β values. Nonetheless, their PR response, as measured by the maximum Δn per unit electric field, exceeds that of all other materials previously described. These chromophores are dominated by charge-resonant properties where, when the linear polarizability (the polarizability anisotropy $\delta\alpha$) is maximized, the first hyperpolarizability is minimized (16).



An important aspect of this PR material design strategy is the multifunctional role that the chromophore plays. Dual-

function dopants (17–19) have been reported previously in which charge transport and optical nonlinearity functions are performed by a single species. Here we report the structures and properties of selected members of a family of dihydropyridines (Table 1) that can be used to formulate organic PR materials in which the chromophore serves as the charge-transporting species, the optically birefringent species and, additionally, acts as the amorphous host. These chromophores are structurally related to the previously described PR chromophore 2,6-dialkyl-4H-pyran-4-ylidenemalononitrile (DPDCP) (15). Exchange of oxygen for nitrogen in the pyran ring produces the dihydropyridine series with enhanced electronic properties and an additional site for functionalization. The compounds with two cyano (malononitrile) acceptor groups examined thus far do not form glasses. Numerous chromophores with other acceptor groups on the 4-ylidene position have been synthesized (20), and differential scanning calorimetry (DSC) (Table 1) showed that cyanoesters had the most pervasive glass-forming properties. Most of the work reported here was done on molecule **4** (*N*-2-butyl-2,6-dimethyl-4H-pyridone-4-ylidene-cyanomethylacetate, 2BNCM) in Table 1, which, at room temperature (near its T_g of 25°C) persists without crystallization. This material should be contrasted with, for example, compound **8**, which exhibits a T_g of 2°C but crystallizes at 57°C. The thermochemical behavior of these systems is complex, and the relation between this behavior and PR is just beginning to be studied.

When a small amount (<1 weight %) of a photosensitizer is added to these glassy monomers, the resulting material exhibits outstanding PR properties such as steady-state Δn in four-wave mixing (FWM) experiments (21) and 2BC gain (22). Their response times are somewhat slower than many of the other PR polymers reported. However, significant increases in the hologram growth rate can be obtained by doping

the chromophore with a small amount of polymer. We have investigated dihydropyridine systems with 10 weight % of polymethylmethacrylate (PMMA), polysiloxane, and PVK, and found each to produce a maximum PR index modulation (at a given applied external field) somewhat lower than the samples without the polymer dopants, but with much faster grating formation speeds. The small amount of polymer did not significantly change T_g . For example, the T_g of a glass formed from 2BNCM and 10% PMMA was reduced by only 3°C.

The steady-state diffraction efficiency η was determined as a function of time and applied electric field E by FWM. The FWM experiments were performed on 150- μ m-thick polymer films sandwiched between two indium tin oxide (ITO) glass plates by using the 676-nm output from a Kr⁺ laser. Details of the sample preparation technique have been described elsewhere (8, 12). The two interfering writing beam external angles were 51° and 71° from the sample normal, and the writing intensity was 1 W/cm². A counterpropagating probe beam with an intensity of 0.007 W/cm² was used to measure η of the holographic gratings formed. We determined Δn from measurements of the p -polarized diffraction efficiency using the expression (4, 10):

$$\eta_p = \sin^2 \left[\frac{\pi d \Delta n \cos(\theta_2 - \theta_1)}{\lambda \sqrt{\cos \theta_1 \cos \theta_2}} \right] \quad (1)$$

where d is the sample thickness, λ the laser wavelength, and θ_1 and θ_2 are the internal angles of incidence of the two writing beams. All measurements were made at room temperature. The time constant for grating formation τ was measured by using FWM for samples containing 90 weight % of the chromophores listed in Table 1 (except for **1** and **5**), 10% PMMA, and 0.3% TNF. The time constants τ were obtained by fitting the initial growth of η_p to the expression:

$$\eta_p(t) = \eta_0(1 - e^{-t/\tau})^2 \quad (2)$$

Table 1. Chromophore structures and properties (R and R' refer to structure in text). A DSC scanning rate of 10°C/min was used to measure T_g , the crystallization temperatures T_c , and the melting points T_m . The decomposition temperature T_{ch} also found from DSC (20°C/min) is well above T_m , which permits processing of the materials from the melt without decomposition.

Compound	R	R'	T_g (°C)	T_c (°C)	T_m (°C)	T_{ch} (°C)
1	Methyl	Methyl			271	385
2	Methyl	Ethyl	35	84	199	377
3	Methyl	1-Propyl	26	67	178, 187	380
4	Methyl	2-Butyl	25		152, 160	351
5	Ethyl	Ethyl	20	66	181	378
6	Ethyl	1-Butyl	8	52, 78	125	385
7	Ethyl	2-Butyl	12	86	123, 138	347
8	Ethyl	2-Ethylhexyl	2	57	105	386

The dark decay was correlated with the growth time constants, with the faster growing samples in general also having a faster dark decay. The slower systems have long dark lifetimes, on the order of several hours. Samples composed of 90% 2BNCM, 9.7% PMMA, and 0.3% TNF were selected for more detailed study in order to assess the potential of these systems for holographic data storage applications, which require long dark lifetimes. The characteristic τ for this system was determined to be 83 s at $E = 40 \text{ V}/\mu\text{m}$. The Kr^+ writing beams interact with a charge-transfer complex (absorption coefficient $\alpha_{676} = 4 \text{ cm}^{-1}$) formed between 2BNCM and TNF. Higher concentrations of TNF lead to stronger PR response but higher absorption losses as well.

Figure 1 shows η_0 as a function of E . Because Δn is proportional to E^2 , $\eta_0(E)$ will have an oscillatory dependence as seen from Eq. 1. The efficiency does not reach 100% at the efficiency maxima because of reflectivity losses at glass/air and glass/PR material interfaces and because of the absorption at this wavelength. The maximum at the second peak is less than the maximum at the first peak because, for the large Δn levels encountered, significant energy is coupled from the probe beam into higher diffraction orders, which are not Bragg matched (23). Table 2 compares the Δn at $40 \text{ V}/\mu\text{m}$ for a number of the best polymeric PR systems. The 2BNCM system is an order of magnitude better in this parameter than any of the systems shown.

In order to verify that a given system is photorefractive a FWM experiment is insufficient, and an experiment such as 2BC must be done, in which the change in the transmitted intensity of two writing beams is recorded as a grating is being formed. An asymmetric exchange of energy between

the two writing beams is a clear indication of a phase-shifted (nonlocal) grating. The increase in intensity of the transmitted beam with gain is measured, and the 2BC gain Γ is obtained from the ratio $\gamma_0 = P_{\text{signal with pump}}/P_{\text{signal without pump}}$, where P_{signal} is the power measured after the sample, from the equation (8):

$$\Gamma = \frac{1}{L} [\ln(\gamma_0\beta) - \ln(\beta + 1 - \gamma_0)] \quad (3)$$

where L is the optical path length for the beam with gain and β is the ratio of write powers incident on the sample. Net internal 2BC gain occurs when Γ exceeds the absorption coefficient α of the material. Table 2 compares the values of Γ and α for several different systems. Again, the net 2BC gain for the 2BNCM system is substantially higher than the values for other systems.

High optical quality of the PR samples is of critical importance for holographic data storage applications. In the organic glass materials reported here, the optical scattering levels are negligible in relation to scattering from the ITO substrates. We have monitored the scattering levels for

samples of both 100% 2BNCM and 90% 2BNCM:9.7% PVK:0.3% TNF maintained at room temperature for more than 90 days without any observable increase in the scattering level, indicating excellent compositional stability, at least during this time period. For longer time periods (>6 months), some samples showed evidence of increased scattering.

As already mentioned, an important potential application for PR materials is in reversible holographic digital optical data storage systems (24, 25). The storage of large numbers of holograms at a single spot in the storage media (multiplexing) can lead to extremely high storage densities. The search for erasable PR holographic storage media (26) has been concentrated on inorganic crystals. Because the additional requirement of high external E fields during the operation of polymeric PR materials limits sample thicknesses to $\sim 100 \mu\text{m}$, the number of holograms that can be multiplexed is smaller than is possible in centimeter-thick inorganic crystals. With the substantially improved performance of the organic glass systems reported here, one does not need to operate

Table 2. Properties of several amorphous organic PR systems at an external field of $40 \text{ V}/\mu\text{m}$. Scattering efficiency was measured at room temperature.

Material	Δn ($\times 10^{-3}$)	Γ (cm^{-1})	α (cm^{-1})	τ^{-1} (s^{-1})	Scattering efficiency
2BNCM*	10	69	4	0.012	0.00022
DMNPAA†	1	25	8	2	0.5
BisA-NAS:DEH‡	0.12	22	105	10	
FDEANST§	0.2	10	17	1	0.05
DTNBI	0.1	28	12	0.0033	0.1
DPDCP¶	0.18	8	2	1	

*0.9 2BNCM:0.1 PMMA:0.003 TNF (this work). †0.5 DMNPAA:0.3 PVK:0.2 ECZ:0.01 TNF (10). ‡BisA-NAS, bisphenol-A-diglycidylether-4,4'-nitroaminostilbene; DEH, diethylaminobenzaldehyde-diphenylhydrazone (7). §0.3 FDEANST:0.7 PVK:0.01 TNF; FDEANST, 3-fluoro-4-*N,N'*-diethylamino- β -nitrostyrene (8). ||0.7 DTNBI:0.3 PMMA:0.03 C_{60} ; DTNBI, 1,3-dimethyl-2,2-tetramethylene-5-nitrobenzimidazole (17, 18). ¶0.3 DPDCP:0.15 TPD:0.55 PMMA:0.3 C_{60} ; TPD, *N,N'*-bis(3-methylphenyl)-*N,N'*-bis(phenyl)benzidine (15).

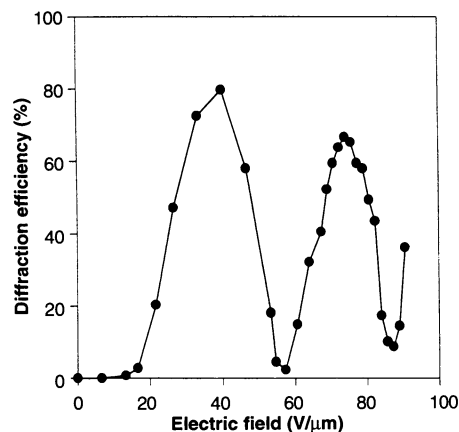


Fig. 1. Steady-state diffraction efficiency (η_0 from Eq. 2) at 676 nm as a function of applied electric field for a 90% 2BNCM; 10% PMMA; 0.3% TNF sample of thickness $150 \mu\text{m}$.

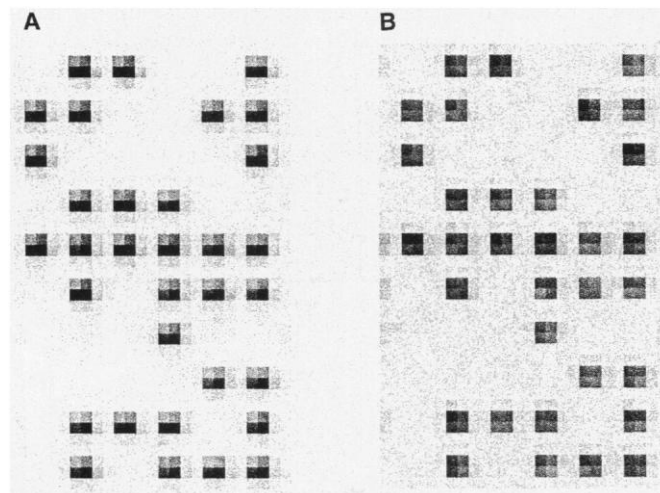


Fig. 2. (A) An image of the digital data recorded on a CCD camera after transmission through the sample. (B) The reconstructed hologram of the digital data of (A) recorded in the sample.

at the highest E fields, thus permitting the use of thicker samples.

We have measured data storage error rates in a holographic optical storage test stand (27–29). Here a coherent 676-nm, data-containing object beam is intersected with a plane-wave reference beam in the PR sample (90% 2BNM, 9.7% PMMA, 0.3% TNF) and a hologram is formed. A portion of a 64-kbit random data page is shown in Fig. 2. The size of each data bit on the mask was 18 μm by 18 μm , and each bit was surrounded by a 9 μm thick, opaque boarder with an overall pitch of 36 μm by 36 μm . The coherent object beam is passed through the data page mask containing the information as just described and focused on the sample to a 4-mm-diameter spot. The hologram is read back by illuminating the sample with only the reference beam and the reconstructed hologram recorded on a charge-coupled device (CCD) detector array. Experiments involved the storage, retrieval, and subsequent erasure of digital data pages with a data density of 0.5 Mbit/cm². For the amorphous glass system described here, single data pages could be stored and retrieved without error using only 1 part in 10⁶ of the total dynamic recording range (that is, Δn range). Holograms were read back periodically at room temperature in air for up to 6 hours with no observable degradation in hologram quality or bit error rate.

The vanishingly small scattering levels in these glasses reduce the hologram efficiency required for error-free readout by a factor of 10 compared with polymeric systems studied previously. Of perhaps equal importance is the extremely large recording dynamic range available in these dihydropyridine systems. The overmodulation of the holographic efficiency, occurring at relatively small E fields (see Fig. 1), means that the smaller field can be applied to thicker samples, increasing the Bragg sensitivity, the number of holograms that can be multiplexed, and the overall hologram quality. In relation to existing polymeric PR systems, these organic glasses would appear to offer substantial advantages.

REFERENCES AND NOTES

- P. Günter and J. P. Huignard, *Photorefractive Materials and Their Applications* (Springer, Berlin, 1988 and 1989), vols. 1 and 2.
- M. Eich *et al.*, *J. Opt. Soc. Am. B* **6**, 1590 (1989); R. J. Twieg and C. W. Dirk, in *Science and Technology of Organic Thin Films for Waveguiding Nonlinear Optics*, F. Kajzar and J. Swalen, Eds. (Gordon and Breach, Newark, NJ, 1996).
- A. Ashkin *et al.*, *Appl. Phys. Lett.* **9**, 72 (1966); F. S. Chen, *J. Appl. Phys.* **38**, 3418 (1967).
- S. Ducharme, J. C. Scott, R. J. Twieg, W. E. Moerner, *Phys. Rev. Lett.* **66**, 1846 (1991).
- W. E. Moerner and S. M. Silence, *Chem. Rev.* **94**, 127 (1994).
- Y. Zhang, R. Burzynski, S. Ghosal, M. Casstevens, *Adv. Mater.* **8**, 111 (1996); L. Yu, W. K. Chan, Z. Peng, A. Gharavi, *Acc. Chem. Res.* **29**, 13 (1996).
- M. Liphardt *et al.*, *Science* **263**, 367 (1994).
- M. C. J. M. Donckers *et al.*, *Opt. Lett.* **18**, 1044 (1993).
- O. Zobel, M. Eckl, P. Strohriegel, D. Haarer, *Adv. Mater.* **11**, 911 (1995).
- K. Meerholtz, B. L. Volodin, Sandalphon, B. Kippelin, N. Peyghambarian, *Nature* **371**, 497 (1994).
- K. Meerholtz, Sandalphon, B. L. Volodin, B. Kippelin, N. Peyghambarian, *Conf. Lasers Electro-Opt. Tech. Dig.* **9**, 497 (1996).
- C. Poga *et al.*, *Proc. Photo.-Opt. Instrum. Eng.* **2526**, 82 (1995).
- A. M. Cox *et al.*, *Appl. Phys. Lett.* **68**, 2801 (1996).
- W. E. Moerner, S. M. Silence, F. Hache, G. C. Bjorklund, *J. Opt. Soc. Am. B* **11**, 320 (1994).
- R. Wortmann *et al.*, *J. Chem. Phys.*, in press.
- S. R. Marder, D. N. Beratan, L.-T. Cheng, *Science* **252**, 103 (1991).
- S. M. Silence *et al.*, *J. Phys. Chem.* **99**, 4096 (1995).
- S. M. Silence, R. J. Twieg, G. C. Bjorklund, W. E. Moerner, *Phys. Rev. Lett.* **73**, 2047 (1994).
- Y. Zhang, S. Ghosal, M. K. Casstevens, R. Burzynski, *Appl. Phys. Lett.* **66**, 256 (1995).
- I. Belsky, H. Dodiuk, Y. Shvo, *J. Org. Chem.* **39**, 989 (1974).
- W. E. Moerner *et al.*, *Proc. Soc. Photo-Opt. Instrum. Eng.* **1564**, 278 (1991).
- C. A. Walsh and W. E. Moerner, *J. Opt. Soc. Am. B* **9**, 1642 (1992); *ibid.* **10**, 753 (1993).
- B. L. Volodin *et al.*, *Opt. Lett.* **21**, 519 (1996).
- F. S. Chen, J. T. LaMacchia, D. B. Frazer, *Appl. Phys. Lett.* **13**, 223 (1968).
- J. F. Heanue, M. C. Bashaw, L. Hesselink, *Science* **265**, 749 (1994).
- P. van Heerden, *Appl. Opt.* **2**, 393 (1963).
- M.-P. Bernal *et al.*, *ibid.* **35**, 2360 (1996).
- P. M. Lundquist *et al.*, *Opt. Lett.* **12**, 890 (1996).
- C. Poga *et al.*, *Appl. Phys. Lett.* **69**, 1047 (1996).
- We thank M.-P. Bernal, H. Coufal, R. K. Grygier, J. A. Hoffnagle, C. M. Jefferson, R. M. Macfarlane, R. M. Shelby, G. T. Sincerbox, P. Wimmer, and G. Wittmann for assistance in using the holographic optical storage test stand. Supported in part by ARPA contracts DAAB07-91-C-K767 and MDA972-94-20008.

9 August 1996; accepted 8 October 1996

Modulation of Insulin Activities by Leptin

Batya Cohen, Daniela Novick, Menachem Rubinstein*

Leptin mediates its effects on food intake through the hypothalamic form of its receptor OB-R. Variants of OB-R are found in other tissues, but their function is unknown. Here, an OB-R variant was found in human hepatic cells. Exposure of these cells to leptin, at concentrations comparable with those present in obese individuals, caused attenuation of several insulin-induced activities, including tyrosine phosphorylation of the insulin receptor substrate-1 (IRS-1), association of the adapter molecule growth factor receptor-bound protein 2 with IRS-1, and down-regulation of gluconeogenesis. In contrast, leptin increased the activity of IRS-1-associated phosphatidylinositol 3-kinase. These *in vitro* studies raise the possibility that leptin modulates insulin activities in obese individuals.

Leptin, an adipocyte-derived cytokine that regulates body weight, was identified by positional cloning of the murine *obese* (*ob*) gene (1) and was shown to affect both food intake and thermogenesis (2). High-affinity leptin-binding sites were detected in the choroid plexus, which led to identification of the leptin receptor OB-R (3). The known activities of leptin are mediated through the hypothalamic OB-R, but OB-R and OB-R variants derived from alternative splicing are expressed in other tissues, notably the kidney, lung, and liver (3–5). This receptor expression pattern suggests that, in addition to control of food intake and body heat, leptin may have other physiological functions. Although leptin is produced by adipocytes, the recent finding that excess fat correlates with high concentrations of leptin in serum (6), and the well-established linkage between obesity and insulin

resistance (7), led us to explore the possibility that leptin may modulate insulin-regulated responses.

To test for possible effects of leptin on insulin-regulated responses, we looked for cell lines expressing a functional OB-R. Various human cell lines derived from liver, lung, and kidney were screened by reverse transcription-polymerase chain reaction (RT-PCR) with oligonucleotides corresponding to the region encoding the extracellular domain of human OB-R (huOB-R) (3). The human hepatocellular carcinoma cell lines HepG2 and Hep3B provided one PCR product whose identity with huOB-R mRNA was confirmed by DNA sequencing. Additional RT-PCR was done with primers corresponding to specific 3' end regions of the four known splice variants of huOB-R. Only one splice variant, with a short cytoplasmic domain (the B219.3–OB-R mRNA) (5), was detected in HepG2 cells. The same product was obtained when RT-PCR was done with mRNA from human liver (Fig. 1A), and its identity was confirmed by sequencing. Northern blot anal-

Department of Molecular Genetics, The Weizmann Institute of Science, Rehovot 76100, Israel.

*To whom correspondence should be addressed. E-mail: lvrub@weizmann.weizmann.ac.il